Title

Dual targeting agents for Aβ plaque/P-glycoprotein and Aβ plaque/nicotinic acetylcholine α4β2* receptors—potential approaches to facilitate Aβ plaque removal in Alzheimer's disease brain

Journal

Medicinal Chemistry Research, 27(6)

ISSN

1054-2523

Authors

Samra, Gurleen K
Dang, Kenneth
Ho, Heather
et al.

Publication Date

2018-06-01

DOI

10.1007/s00044-018-2178-9

Peer reviewed

HHS Public Access

Author manuscript

Med Chem Res. Author manuscript; available in PMC 2019 June 01.

Published in final edited form as:

Med Chem Res. 2018 June ; 27(6): 1634–1646. doi:10.1007/s00044-018-2178-9.

Dual targeting agents for Aβ plaque/P-glycoprotein and Aβ plaque/nicotinic acetylcholine α4β2* receptors—potential approaches to facilitate Aβ plaque removal in Alzheimer's disease brain

Gurleen K. Samra[1], **Kenneth Dang**[1], **Heather Ho**[1], **Aparna Baranwal**[1,3], and **Jogeshwar Mukherjee**[1,2]

[1]Preclinical Imaging, Department of Radiological Sciences, University of California-Irvine, Irvine, CA 92697, USA

[2]Department of Biomedical Engineering, University of California-Irvine, Irvine, CA 92697, USA

Abstract

Alzheimer's disease (AD) affects 10% of people older than 65 and is characterized by a progressive loss of cognitive function with an abnormal accumulation of amyloid β (Aβ) plaques and neurofibrillary tangles (NFT) in the brain. Efforts to reduce brain Aβ plaques continue to be investigated as a therapeutic approach for AD. We report here development of dual targeting agents with affinity for Aβ plaque/P-glycoprotein (Pgp) and Aβ plaque/α4β 2* nicotinic acetylcholine receptors (nAChR). These novel dual agents may be able to efflux Aβ plaques via the paravascular (glymphatic) pathways. Ferulic acid (FA), ferulic acid ethyl ester (FAEE), and curcumin (CUR) were used for Aβ plaques, fexofenadine (FEX) was used as substrate for Pgp and nifrolidine (NIF) was used for α4β 2* nAChRs. Aβ plaque/α4β 2* nAChR dual agent, FA-NIF (GKS-007) exhibited IC_{50} = 3–6 nM for α4β 2* nAChRs in [^{3}H]cytisine-radiolabeled thalamus and frontal cortex in rat brain slices. In postmortem human AD frontal cortex, Aβ plaques labeled with [^{3}H]PIB, FEX-CUR showed a 35% reduction in gray matter (GM)/white matter (WM) [^{3}H]PIB binding, while CUR alone showed a 50% reduction. In vivo biodistribution studies are required of the Aβ-Pgp and Aβ-α4β 2* nAChRs dual targeting agents in order to evaluate their potential as therapeutic approaches for reducing brain Aβ plaques.

Graphical Abstract

[3]Present address: West Virginia School of Osteopathic Medicine, Lewisburg, WV, USA

Compliance with ethical standards

Conflict of interest

The authors declare that they have no conflict of interest.

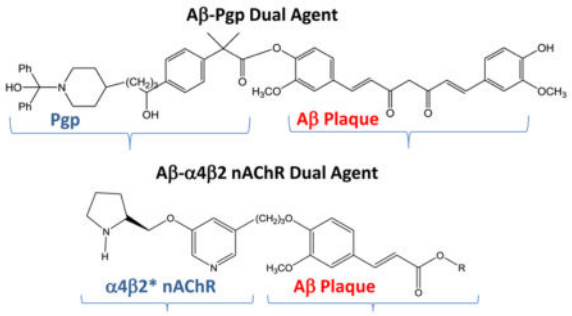

Keywords

Alzheimer's disease; Plaque removal; Ferulic acid; Curcumin; Nifene; PET imaging

Introduction

Alzheimer's disease (AD) is a neurodegenerative disease characterized by the accumulation of β-amyloid plaques (or senile plaques, SP) and neurofibrillary tangles (NFT) in the brain (Braak and Braak 1991). Over the last few years efforts on diagnostic methods for plaques and more recently on NFT using positron emission tomography (PET) have made significant progress (Ariza et al. 2015). With increasing efforts to find treatments and cure for AD, imaging plaques and NFT can contribute to the diagnosis and clinical management of AD (Barten and Albright 2008; Moghbel et al. 2012). Emphasis is now on finding improved treatment strategies for AD. Currently, the only FDA approved drugs for AD treatment include acetylcholinesterase inhibitors (AChEI), such as donepezil, which may be supplemented with memantine (or Namenda) (#1 in Table 1). These drugs lessen symptoms of memory loss and confusion.

Reduction in the accumulation of amyloid β (Aβ) plaques and NFT continues to be investigated as therapeutic approaches for AD (Tampellini 2015; Venigalla et al. 2016). Although, the NFT hypothesis is being sought after as a better indicator of clinical AD, Aβ plaque is still being pursued and efforts have been made to remove Aβ plaques in AD patients using antibodies (Salloway et al. 2014; Doody et al. 2014). Current approaches underway as AD treatments involve attempts to decrease the plaque load in the brain either by removal of the Aβ plaques (using antibodies, curcumin (CUR) analogs and ultrasound) or decrease the production (using secretase inhibitors) of the Aβ plaques in the brain (Table 1). Large clinical trials were carried out with anti-amyloid monoclonal antibodies, bapineuzumab (#2 Table 1; Salloway et al. 2014) and solanezumab (#3 Table 1; Doody et al. 2014; Siemers et al. 2016). Both of these trials did not improve clinical outcome and importantly the Aβ plaque load (measured by PET imaging) did not change significantly before and after antibody treatment. A different approach currently underway is to reduce the production of Aβ peptide by inhibition of the two secretases enzymes (- and β -), which cleave the amyloid precursor protein (APP; #4 Table 1). The -secretase inhibitors have an adverse effect on notch signaling pathway and were therefore not found to be suitable for further development. Development of β-secretase inhibitors are being pursued (Filser et al.

2015), although some of them have been discontinued due to liver toxicity (Vassar 2014). The natural product CUR and its analogs continue to be investigated for their anti-inflammatory and anti-amyloidogenic properties (#5 Table 1; Hu et al. 2015; Gerenu et al. 2015) but concerns remain about efficacy in humans and brain bioavailability.

Transgenic mice have considerably accelerated the understanding of the mechanisms of neurodegeneration underlying AD and development of therapeutics that may slow, halt, and potentially reverse AD. Immunization with fibrillar Aβ in young transgenic mice overexpressing mutant human APP can prevent subsequent plaque development (Schenk et al. 1999). A number of therapeutic agents have been tested, such as nonsteroidal anti-inflammatory drugs, antioxidants, and statins in transgenic mice. Although, they provide insights on AD treatment, translation to humans has not occurred. More recently, scanning ultrasound was repeatedly used on the mouse brain to make the blood–brain barrier (BBB) leaky for Aβ removal (#6 Table 1; Leinenga and Gotz 2015). Adaptation of this method to human use may pose a challenge. No efforts to remove Tau products from the brain have been made to the best of our knowledge.

Our overall goal is to develop dual targeting agents consisting of an Aβ plaque target agent that will be linked to a second target agent to assist in removal of the plaque from the brain and surrounding vasculature (Fig. 1). P-glycoprotein (Pgp) is known to efflux macromolecules across the BBB and blood-cerebrospinal fluid barrier (BCSF; Jessen et al. 2015). One specific objective is to develop and evaluate dual targeting agents with substrate affinity for Pgp and high affinity for Aβ plaque (Pgp-Aβ-binding molecule) that may be able to bind to Aβ and be effluxed out of the brain by Pgp using the paravascular (or glymphatic) pathways and olfactory lymphatic pathways (Fig. 1b; Bacyinski et al. 2017; Krishnamurthy et al. 2014). In order to obtain a suitable dual Pgp-Aβ-binding agent, three features will be incorporated: (1) use ferulic acid (FA) **2** and CUR **3** as Aβ-binding agents; (2) Use fexofenadine (FEX) **4** (Tahara et al. 2005) as the substrate for Pgp; (3) use a linker 1-amino-4-butanol to connect the two targeting molecules. Ferulic acid ethyl ester (FAEE) and FA (**1** and **2**, Fig. 2), which are hemi-analogs of CUR **3** have all been reported to have anti-amyloidogenic properties.

The second approach is anchoring Aβ plaque clearing agents using neuronal α4β 2* nicotinic acetylcholine receptors (nAChRs) and thus prolong their residence time in specific brain regions (Fig. 1d). The α4β 2* nAChRs receptors are involved in learning and memory and have been implicated in human neurodegeneration, including Alzheimer's disease, Parkinson's disease (Posadas et al. 2013). The α4β 2* nAChRs are localized in frontal cortex, cingulate, temporal cortex, subiculum, and parts of the hippocampus, all of which are known to have significant amounts of Aβ plaques in AD patients. We have previously prepared fluoroalkyl derivatives such as nifrolidine (NIF) **5** as radioligands for α4β 2* receptors (Chattopadhyay et al. 2005; Pichika et al. 2011, 2013). Derivatization of the 3-carbon chain at the 5-position in NIF does not adversely affect their binding to the α4β 2* nAChRs as reported in our recent work for fluorescent probes containing large fluorophores at the 5-position (Samra et al. 2018). Thus, NIF derivative was coupled to FAEE and FA to provide the second class of dual targeting agents.

Thus, in this paper we report the following: (1) synthesis of dual Aβ-Pgp-binding agent using FEX (Fig. 2) as the substrate for Pgp (Tahara et al. 2005) and FA and CUR as Aβ-binding agents; (2) synthesis of dual Aβ-α4β 2* nAChR-binding agent using NIF backbone (Chattopadhyay et al. 2005) for α4β 2* nAChR (Fig. 2) and FAEE and FA as Aβ-binding agents; (3) measurement of in vitro competition of the dual agents with [^{3}H]PIB labeled Aβ plaques in postmortem human AD brain slices. (4) Measurement of in vitro binding affinities of Aβ-α4β 2* nAChR agents in rat brain slices using [^{3}H]cytisine labeled α4β 2* nAChR sites.

Materials and methods

General methods

All chemicals and solvents were of analytical or high performance liquid chromatography (HPLC) grade from Aldrich Chemical Co. and Fisher Scientific. Electrospray mass spectra were obtained on a Model 7250 mass spectrometer (Micromass LCT). Proton nuclear magnetic resonance (NMR) spectra were recorded on a Bruker OMEGA 600 MHz spectrometer. Analytical thin layer chromatography (TLC) was carried out on silica coated plates (Baker-Flex, Phillipsburg, NJ). Chromatographic separations were carried out on preparative TLC (silica gel GF 20 × 20 cm 2000 micron thick; Alltech Assoc. Inc., Deer-field, IL) or silica gel flash columns or semi-preparative reverse-phase columns using the Gilson HPLC systems. Rat and human postmortem brain slices were obtained on a Leica 1850 cryotome. [^{3}H]Cytisine and [^{3}H]PIB autoradiographic studies were carried out by exposing tissue samples on storage phosphor screens. The apposed phosphor screens were read and analyzed by OptiQuant acquisition and analysis program of the Cyclone Storage Phosphor System (Packard Instruments Co., Boston, MA). All rodent studies were approved by the Institutional Animal Care and Use Committee (IACUC) of the University of California, Irvine. All human postmortem brain tissue studies were approved by the Institutional Biosafety Committee of the University of California, Irvine.

Synthesis

Ethyl 3-methoxy-4-(1′-N-BOC-aminobutyryloxy)cinnamate 6—Ethyl ferulate **1** (45 mg; 0.2 mmol) was dissolved in tetra-hydrofuran (1 mL). To this solution, potassium *tert*-but-oxide (50 mg) was added at room temperature and stirred for 15 min followed by the addition of *N*-BOC-4-bromo-butan-1-amine (51 mg; 0.2 mmol) was added. The solution turned bright yellow and was stirred at room temperature for 24 h. The reaction was then washed with saturated sodium bicarbonate and extracted with dichloromethane. The organic extract was puriied on preparative silica gel TLC using 9:1 dichloromethane-methanol to provide 37 mg (~45% yield) of pure **6**. Mass spectra (m/z, %): 394 ([M + H]$^+$, 10%), 416 ([M + Na]$^+$, 25%), 809 ([2 M + Na]$^+$, 100%). 1 H NMR ($CDCl_3$, 600 MHz) δ p.p.m.: 7.54 (d, 2 H, J = 15.9 Hz), 7.05 (d, 1 H, J = 8.2 Hz), 6.77 (d, 1 H, J = 8.2 Hz), 6.23 (d, 1 H, J = 15.9 Hz), 4.19 (m, 2 H, OCH_2), 3.97 (m, 2 H), 3.82 (s, 3 H, OCH_3), 3.12 (m, 2 H), 1.82 (m, 2 H), 1.62 (m, 2 H), 1.37 (s, 9 H, *N*-BOC), and 1.28 (t, 3 H, CH_3).

Ethyl 3-methoxy-4-(1′-aminobutyryloxy)cinnamate 7—The *N*-BOC derivative **6** (20 mg; 50 μmol) was taken in dichloromethane (2 mL) into which 0.1 mL of trifluoroacetic

acid (TFA) was added. The reaction was stirred at room temperature for 24 h. The reaction was quenched with saturated sodium bicarbonate and extracted with dichloromethane. The organic extract was purified on preparative silica gel TLC using 9:1 dichloromethane-methanol to provide 14 mg (~95% yield) of pure **7**. Mass spectra (m/z, %): 294 (100%, $[M + H]^+$). 1 H NMR ($CDCl_3$, 600 MHz) δ p.p.m.: 7.62 (d, 2 H, *J* = 15.9 Hz), 7.08 (d, 1 H, *J* = 8.2 Hz), 6.84 (d, 1 H, *J* = 8.2 Hz), 6.31 (d, 1 H, *J* = 15.9 Hz), 4.26 (m, 2 H, OCH_2), 4.09 (br, 2 H), 3.82 (s, 3 H, OCH_3), 3.11 (br, 2 H), 1.90-2.05 (br, 4 H), and 1.34 (t, 3 H, CH_3).

FEX-(3-methoxy-4-(1′-aminobutyryloxy)cinnamic acid 8—FEX **4** (13 mg; 26 μmol) was dissolved in acetonitrile (2 mL). To this solution, amine **7** (10 mg; 34 μmol) was added followed by addition of BOP (15 mg; 34 μmol) along with 0.1 mL triethylamine. The mixture was stirred at room temperature for 24 h. The reaction solvent was removed and the residue was taken up in dichloromethane and washed with saturated sodium bicarbonate. The organic layer was dried and purified on preparative silica gel TLC using 9:1 dichloromethane-methanol to provide 11 mg (~54% yield) of pure amide in >95%. Mass spectra (m/z, %): 777 ($[M + H]^+$, 55%). This amide was taken in methanol (0.5 mL) into which 0.5 mL of 1 N sodium hydroxide was added. The reaction mixture was heated at 60 ^oC for 30 min. The reaction was quenched with water and extracted with dichloromethane. The organic extract was purified on preparative silica gel TLC using 1:1 dichloromethane-methanol to provide pure **8**. Mass spectra (m/z, %): 749 ($[M + H]^+$, 20%). 1 H NMR ($CDCl_3$, 600 MHz) δ p.p.m.: 7.62 (d, 2 H, J = 15.9 Hz), 7.50 (m, 4 H), 7.28–7.35 (br, 8 H), 7.20–7.13 (m, 2 H), 6.84 (d, 1 H, J = 8.2 Hz), 6.36 (d, 1 H, J = 15.9 Hz), 4.09 (br, 2 H), 3.82 (s, 3 H, OCH_3), 3.50 (m, 2 H), 3.11 (br, 2 H), 3.01 (m, 3 H), 2.93 (m, 2 H), 1.90-2.05 (br, 4 H), 1.72 (br, 8 H), and 1.52 (6 H, m).

FEX curcuminate 9

FEX **4** (26.9 mg; 54 μmol) was dissolved in acetonitrile (2 mL). To this solution, CUR **3** (18.6 mg; 50 μmol) was added followed by addition of BOP (23 mg; 52 μmol) along with 0.1 mL triethylamine. The solution turned bright orange and was stirred at room temperature for 24 h. The reaction solvent was removed and the residue was taken up in dichloromethane and washed with saturated sodium bicarbonate. The organic layer was dried and purified on preparative silica gel TLC using 9:1 dichloromethane-methanol to provide pure **9** in >90% purity with an approximate yield of 25%. Mass spectra (m/z, %): 875 ([M + Na]+, 30%). NMR ($CDCl_3$, 600 MHz) δ 7.62 (2 H, m), 7.50 (2 H, m), 7.33–7.39 (14 H, m), 7.23 (2 H, m), 7.11 (2 H, m), 6.51 (2 H, d, *J* = 15.7 Hz), 5.24 (1 H, s), 4.64 (1 H, d,), 3.81 (3 H, s), 3.79 (3 H, s), 3.50 (2 H, m), 3.01 (3 H, m), 2.93 (2 H, m), and 1.63–1.77 (14 H, m).

5-(3′-Ethyl 3-methoxy-4-propyloxycinnamate)-3-(1-BOC-2-(S)-pyrrolidinylmethoxy)pyridine 11—5-(3-Tosyloxypropyl)-3-(1-BOC-2-(*S*)-pyrrolidinylmethoxy)pyridine **10** (34 mg, 70 μmol; prepared previously (Chattopadhyay et al. 2005) was reacted with ethyl ferulate **1** (20 mg, 90 μmol) in dimethylformamide (1 mL) in the presence of potassium *tert*-butoxide (12 mg). The reaction was heated for 24 h at 100 °C and subsequently water (2 mL) was added and the mixture was extracted with dichloromethane. The dichloromethane extract was purified on preparative silica gel TLC using 9:1 dichloromethane-methanol to provide **11** in >95% purity and a yield of ~30%. Mass spectra

(m/z, %), 541 ([M + H]$^+$, 100%), 563 ([M + Na]+, 90%). NMR ($CDCl_3$, 600 MHz) δ p.p.m.: 8.10 (s, 1 H), 8.04 (s, 1 H), 7.62 (d, 2 H, *J* = 15.9 Hz), 7.60 (s, 1 H), 7.07 (d, 1 H, *J* = 8.2 Hz), 7.04 (s, 1 H), 6.92 (d, 1 H, *J* = 8.2 Hz), 6.30 (d, 2 H, *J* = 15.9 Hz), 4.26 (m, 2 H, OCH_2), 4.11 (m, 2 H), 3.95 (m, 1 H), 3.65 (m, 2 H), 3.39 (m, 2 H), 3.93 (s, 3 H, OCH_3), 2.78 (m, 2 H), 1.99 (m, 6 H), 1.47 (s, 9 H, *N*-BOC), and 1.27 (s, 3 H, CH_3).

5-(3′-Ethyl 3-methoxy-4-propyloxycinnamate)-3-(2-(S)-pyrrolidinylmethoxy)pyridine 12—The substituted ethyl ferulate **11** (5 mg; 9 μmol) was taken in dichloromethane (1 mL) into which 0.1 mL of TFA was added. The reaction was stirred at room temperature for 24 h. The reaction was quenched with saturated sodium bicarbonate and extracted with dichloromethane. The organic extract was purified on preparative silica gel TLC using 9:1 dichloromethane-methanol to provide pure **12**. Mass spectra (m/z, %), 413 ([M + H]$^+$, 75%). NMR (CD_3OD, 600 MHz) δ p.p.m.: 8.13 (s, 1 H), 8.06 (s, 1 H), 7.62 (d, 2 H, *J* = 15.9 Hz), 7.60 (s, 1 H), 7.05 (d, 1 H, *J* = 8.2 Hz), 7.02 (s, 1 H), 6.92 (d, 1 H, *J* = 8.2 Hz), 6.30 (d, 2 H, *J* = 15.9 Hz), 4.27 (m, 2 H, OCH_2), 4.15 (m, 2 H), 3.95 (m, 1 H), 3.91 (s, 3 H, OCH_3), 3.65 (m, 2 H), 3.39 (m, 2 H), 2.78 (m, 2 H), 1.99 (m, 6 H), and 1.27 (s, 3 H, CH_3).

5-(3-methoxy-4-propyloxycinnamate)-3-(2-(S)-pyrrolidinylmethoxy)pyridine 13—Ether **12** (4 mg; 10 μmol) was taken in methanol (0.5 mL) into which 0.5 mL of 1 N sodium hydroxide was added. The reaction mixture was heated at 60 °C for 30 min. The reaction was quenched with water and extracted with dichloromethane. The organic extract was purified on preparative silica gel TLC using 1:1 dichloromethane-methanol to provide pure **13**. Mass spectra (m/z, %), 441 ([M + H]$^+$, 100%). NMR (CD_3OD, 600 MHz) δ p.p.m.: 8.17 (s, 1 H), 8.06 (s, 1 H), 7.62 (d, 2 H, *J* = 15.9 Hz), 7.60 (s, 1 H), 7.07 (d, 1 H, *J* = 8.2 Hz), 7.04 (s, 1 H), 6.92 (d, 1 H, *J* = 8.2 Hz), 6.30 (d, 2 H, *J* = 15.9 Hz), 4.15 (m, 2 H), 3.93 (m, 1 H), 3.91 (s, 3 H, OCH_3), 3.70 (m, 2 H), 3.42 (m, 2 H), 2.78 (m, 2 H), and 1.99 (m, 6 H).

In vitro studies

All animal studies were approved by the IACUC of the University of California-Irvine. Ex vivo rat brain slices were prepared at 10 μm thick using a Leica 1850 cryotome and used for [^{3}H]cytisine binding. Autoradiographic studies using [^{3}H]cytisine and drug (GKS-006 and GKS-007) concentrations were carried out by exposing tissue radi-olabeled brain sections on storage phosphor screens (Perkin Elmer Multisensitive, Medium MS). The apposed phosphor screens were read and analyzed by OptiQuant acquisition and analysis program of the Cyclone Storage Phosphor System (Packard Instruments Co., Boston, MA). Region-of-interest (ROI) of same size were drawn and analyzed on brain regions using OptiQuant software and binding of [^{3}H] cytisine measured in Digital Light Units/mm^2 (DLU/mm^2). Data was analyzed using following procedure: (1) the nonspecific binding of [^{3}H]cytisine was subtracted for all samples; (2) the specific binding was normalized to 100% (no competitive ligand), and (3) the binding isotherms were fit to the Hill equation (KELL BioSoft software (v 6), Cambridge, UK).

Using our previously described procedure on [^{3}H]PIB,[25] postmortem human AD frontal cortex sections (10 μm thick; human brain tissue obtained from Banner Sun Health Research Institute, Sun City, AZ) were preincubated in 10% alcohol PBS buffer for 10 min. The brain sections were placed in a glass chamber and incubated with [^{3}H]PIB (2 μCi/cc) in 10% alcohol PBS buffer, pH 7.4 at 37 °C for 1 h. The slices were then washed with cold 10% alcohol PBS buffer (2 × 3 min), cold deionized water 1 min, respectively. The brain sections were air dried, exposed overnight on a phosphor film, and then placed on the Phosphor Autoradiographic Imaging System/Cyclone Storage Phosphor System (Packard Instruments Co). ROIs were drawn on the slices and the extent of binding of [^{3}H]PIB was measured with DLU/mm^2 using the OptiQuant acquisition and analysis program (Packard Instruments Co).

Results

Synthesis

For Pgp and Aβ amyloid dual agent, two different approaches were taken. Figure 3 shows derivatization of FAEE with the 4-carbon linker. In the presence of base, the phenolate of FAEE **1** was reacted with *N*-BOC-1-bromo-4-butylamine to provide **6** in 45% yield. Removal of the *N*-BOC protecting group using TFA resulted in the corresponding amine **7** in 95% yields. FEX **4** was coupled to the amine **7** using BOP to form the amide derivative of FAEE. Base hydrolysis of this amide-ester resulted in the FA derivative **8** in 50–60% yields.

The second approach for Pgp and Aβ amyloid dual agent is shown in Fig. 4. FEX **4** was directly coupled to CUR **3** using BOP to form the FEX-CUR derivative **9** in an ester linkage. This dual agent ester was obtained in moderate yields. Potential steric effects from the adjacent *gem*-dimethyl group may have affected the yields. The use of the 4-carbon linker may help in increasing the coupling yield, with the formation of an ether-amide link between FEX and CUR.

To obtain dual agent for α4β 2* nAChRs and Aβ amyloid, the *N*-BOC tosylate **10** was used, which was synthesized previously.[21] Coupling of the *N*-BOC tosylate **10** with FAEE **1** was carried out using nucleophilic substitution reaction by the phenolate of FAEE shown in Fig. 5. The ether **11** was obtained in 30% yields. Formation of the ether under Mitsunobu reaction conditions using DIAD/Ph_3P as the coupling agent did not provide good yields. Removal of the *N*-BOC protecting group using TFA resulted in GKS-006 **12** in 85–90% yield. Base hydrolysis of the ethyl ester in GKS-006 **12** provided GKS-007 **13** in 80% isolated yields. The purified GKS-006 and GKS-007 were used for in vitro studies.

Aβ plaque binding

The Aβ plaque-Pgp dual agents, KD-003 and CUR-FEX were tested for binding to Aβ amyloid plaques in human postmortem AD brain frontal cortex slices that were labeled with [^{3}H]PIB (75–90 year olds, Braak score V–VI). Figure 6a shows [^{3}H]PIB labeling of human AD frontal cortex section, which was greater in the gray matter (GM) regions compared to white matter (WM) regions with GM/WM ratio of approx. 3. In the presence of FA (10 μM) both GM and WM showed higher levels of [^{3}H]PIB with a GM/WM ratio of 2 (Fig. 6b). The dual agent KD-003 (Fig. 6c, 10 μM) also showed higher levels of [^{3}H]PIB with GM/WM

ratio of 2.4. CUR (10 μM), known to have a high affinity for Aβ amyloid showed the lowest GM/WM ratio of 1.5 (Fig. 6e, g). The dual agent of CUR, CUR-FEX (10 μM) showed lower binding of [^{3}H]PIB (Fig. 6d, f), with GM/WM ratio reduction to 1.96 as seen in Fig. 6g.

The Aβ plaque-α4β 2* nAChR dual agent was tested for binding to Aβ amyloid plaques in human postmortem AD brain frontal cortex slices labeled with [^{3}H]PIB (75–90 year olds, Braak score V–VI). Figure 7b shows [^{3}H]PIB labeling of human AD frontal cortex section (Fig. 7a), which was greater in the GM regions compared to WM regions with GM/WM ratio of ~2. In the presence of 4-methylamino-4'-N,N-dimethylaminoazobenzene (TAZA) (1 μM), which is known to bind to Aβ amyloid plaques with high affinity (Pan et al. 2016), significant displacement of [^{3}H]PIB occurred from the GM regions (Fig. 7c), with GM/WM ratio reducing to 1:3. Unlike the effects of TAZA, FA (1 μM) did not significantly affect the binding of [^{3}H]PIB (Fig. 7d), with GM/WM ratio of ~2, which was similar to that of the control (Fig. 7b). Similarly the Aβ plaque-α4β 2* nAChR dual agent, GKS-007 10 (1 μM) containing FA appeared to have some inhibitory effect on [^{3}H]PIB (Fig. 7e), but there was no significant GM/WM ratio reduction as seen in Fig. 7g.

Nicotinic receptor binding

The Aβ plaque-α4β 2* nAChR dual agents were tested for their affinity to the α4β 2* nAChRs using rat brain slices labeled with [^{3}H]cytisine. Figure 8 shows [^{3}H]cytisine labeling of rat brain regions of thalamus, frontal cortex, striatum, subiculum, and cerebellum as previously reported (Samra et al. 2018). Displacement of significant amounts of [^{3}H]cytisine was observed by 100 nM of GKS-006 (Fig. 8c) and 100 nM GKS-007 (Fig. 8d). Three brain regions analyzed included thalamus, frontal cortex, and subiculum. With increasing concentration of GKS-006 (Fig. 8e, g) and GKS-007 (Fig. 8f, h) binding of [^{3}H]cytisine was reduced from all brain regions. Measured inhibitory constants (IC_50) of GKS-006 in the various brain regions were: thalamus = 2.80 nM; frontal cortex = 5.33 nM; subiculum = 2.83 nM. Similarly, measured inhibitory constants (IC_50) of GKS-007 in the various brain regions were: thalamus = 3.44 nM; frontal cortex = 3.18 nM; subiculum = 5.40 nM.

Discussion

There is an increasing evidence of the presence of ventricular clearance pathways, such as the paravascular (or also referred as glymphatic) pathway and olfactory lymphatic pathway, which may be involved in clearing macromolecules from the brain (Jessen et al. 2015; Bacyinski et al. 2017). Specific proteins, such as aquoporin4, have been identified that may play a critical role in the movement of water containing macromolecules (Jessen et al. 2015). Insufficient clearance of macromolecules, such as Aβ , results in formation of Aβ fibrils and plaques in the brain. Downregulation of Pgp has been reported in AD (Bartels 2011; Pahnke et al. 2008) and upregulation of Pgp using rifampicin and caffeine were found to increase clearance of Aβ from the brain (Qosa et al. 2012). In normal human plasma a soluble form of lipoprotein receptor related protein (LRP1) is a major endogenous brain Aβ “sinker” that sequesters up to 90% of plasma Aβ peptides. In AD the levels and capacity of LRP1 are reduced that increases free Aβ fraction in plasma. This in turn may increase the brain Aβ

burden through decreased Aβ efflux and/or increased Aβ influx across the BBB (Deane et al. 2009). To what extent these efflux pathways along with Pgp may be involved in removal of the larger Aβ products (oligomers, fibrils, and plaques) from the brain is currently not known.

Thus, our first approach was to assist and enhance the ability of Pgp to increase Aβ efflux. Several substrates and inhibitors have been well characterized for Pgp (Syvanen and Eriksson 2013). FEX is an antihistamine used for allergies and is a Pgp substrate (Tahara et al. 2005; Zhao et al. 2009). The presence of the carboxylic acid functional group enables its easier derivatization compared to other Pgp substrates (Fig. 2). Modification of the carboxylic acid end of FEX may not have major detrimental effects on its interaction with Pgp as a substrate. The carboxylic acid group in FEX was used to form either an amide bond to attach a 4-carbon chain linker to FA or alternatively it was attached directly to CUR in a phenolic ester linkage. Energy-minimized structures of FEX, CUR, and the dual agent CUR-FEX exhibited similar backbone structures suggestive of maintenance of binding properties of CUR to Aβ amyloid (Fig. 4). FA, FAEE, and CUR have all been reported to bind and interact with Aβ amyloid plaques and help in the dissolution/disaggregation of the Aβ plaques (Mancuso and Santangelo 2014; Sultana 2012; Sgarbossa et al. 2015; Yan et al. 2013).

In order to enhance this property of dissolution/dis-aggregation of the Aβ plaques by FAEE and FA, our second strategy involved increasing the brain retention time of these agents by anchoring them to a secondary target. Using our previously developed PET imaging agent [^{18}F]NIF, we recently reported two fluorescent probes, nifrodansyl, and nifrofam with nanomolar affinities for α4β 2* nAChRs (Samra et al. 2018). Nifrofam labeling was observed in α4β 2* nAChR-expressing HEK cells and was upregulated by nicotine exposure. Based on these findings, we used a similar approach in derivatizing NIF using a ether linkage (as opposed to an amide linkage in the case of nifrofam) with FAEE and FA. Energy-minimized structures of NIF, FA, and the dual agent FA-NIF (GKS-007) shows retention of primary-binding features to α4β 2* nAChR (Fig. 5). This was confirmed by the high affinity measured for both GKS-006 and GKS-007 at the α4β 2* nAChR sites in rat brain slices.

CUR had a significant displacement effect on the binding of [^{3}H]PIB to the Aβ plaques in human frontal cortex (Fig. 6). This is consistent with the binding affinity for Aβ plaques/fibrils reported for CUR (Ryu et al. 2006). Although, binding of [^{3}H]PIB by 10 μM CUR was reduced by 50%, a higher degree of displacement would have been expected based on the affinity of CUR. It is likely that the affinity of CUR in SP in human postmortem brain slices may be lower. Displacement of [^{3}H]PIB by TAZA (Fig. 7) was greater than observed by CUR and is consistent with our previous findings of the high affinity of TAZA for Aβ plaques (Pan et al. 2016). Compared to both CUR and TAZA, FA exhibited little displacement of [^{3}H]PIB, suggesting weaker affinity for Aβ plaques and is consistent with reported findings of FA. Of the dual agents, CUR-FEX exhibited the largest displacement of [^{3}H]PIB (GM/WM reduced by 35%) because of the greater effect of CUR, compared to KD-003 and GSK-007, which are dual agents for Pgp and α4β 2* nAChR, respectively,

containing FA. It is likely that higher concentrations of FA and the dual agents containing FA may have a greater effect in reducing [^{3}H]PIB binding.

The glymphatic pathway consisting of aquaporin4 along with the receptors for Aβ transport across the BBB from brain to blood LRP1, receptor for advanced glycation end products and Pgp play a major role in the efflux of Aβ (Bacyinski et al. 2017; Deane et al. 2009). Crystal structure of Pgp at 3.8 Å revealed an internal cavity of ~6000 Å cubed with a 30 Å separation of the two nucleotide-binding domains. Two additional Pgp structures with cyclic peptide inhibitors demonstrate distinct drug-binding sites in the internal cavity capable of stereoselectivity that is based on hydrophobic and aromatic interactions (Aller et al. 2009). Based on this size, the Pgp pore may not directly efflux large Aβ products, but we anticipate that Aβ-Pgp dual agents may assist in the bringing Aβ products in the vicinity of BBB and BCSF in order for the glymphatic pathway to efflux the macromolecules. Additionally if smaller fragments of Aβ fibrils are formed by the action of CUR containing dual agent (Garcia-Alloza et al. 2007), they may be taken across the BBB more efficiently.

Further evaluation will require measurement of Pgp substrate selectivity of the Aβ-Pgp dual agents; preparation of the higher affinity CUR derivative, CUR-NIF so that it has a high affinity for both the α4β 2* nAChRs and Aβ plaques. In vivo studies in transgenic mice (e.g., Coleman et al. 2017; Pi et al. 2012) are planned with both classes of dual agents in order to evaluate stability, BBB permeability and interaction with the target sites for α4β 2* nAChRs (Mukherjee et al. 2018), Aβ plaques (Brendel et al. 2015), and Pgp (Vlaming et al. 2015).

Conclusions

We have successfully developed two classes of dual targeting agents, Aβ plaque/Pgp and Aβ plaque/α4β 2* nAChR in an effort to provide novel approaches to help remove Aβ plaques from the AD brain. Preliminary findings show that both classes of compounds maintain affinity for their respective targets. Further in vitro and in vivo studies are needed to fully characterize them and validate their potential to bind to Aβ plaques, including fibrils in the brain and surrounding vasculature.

Acknowledgments

This research was financially supported by a grant from NIH/NIA AG029479 (J.M.). We like to thank Banner Sun Health Research Institute, Sun City, Arizona for the postmortem human brain tissue samples, and Christopher Liang for technical assistance.

References

Aller SG, Yu J, Ward A, Weng Y, Chittaboina S, Zhuo R, Harrell PM, Trinh YT, Zhang Q, Urbatsch IL, Chang G. Structure of P-glycoprotein reveals a molecular basis for poly-specific drug binding. Science. 2009; 323:1718–1722. [PubMed: 19325113]

Ariza M, Kolb HC, Moechars D, Rombouts F, Andres JI. Tau positron emission tomography (PET) imaging: past, present, and future. J Med Chem. 2015; 58:4365–4382. [PubMed: 25671691]

Braak H, Braak E. Neuropathological staging of Alzheimer-related changes. Acta Neuropathol. 1991; 82:239–259. [PubMed: 1759558]

Bartels AL. Blood brain barrier P-glycoprotein function in neurodenerative disease. Curr Pharm Des. 2011; 17:2771–2777. [PubMed: 21831040]

Baranwal A, Patel HH, Mukherjee J. [18F]Fluorodeox-yglycosylamines: Maillard reaction of ^{18}F-FDG with biological amines. J Label Compds Radiopharm. 2014; 57:86–91.

Barten DM, Albright CF. Therapeutic strategies for Alzheimer's disease. Mol Neurobiol. 2008; 37:171–186. [PubMed: 18581273]

Bacyinski A, Xu M, Wang W, Hu J. The paravascular pathway for brain waste clearance: current understanding, significance and controversy. Front Neuroanat. 2017; 11:101. [PubMed: 29163074]

Brendel M, Jaworska A, Greissinger E, Rotzer C, Burgold S, Gildehaus FJ, Carlsen J, Cumming P, Baumann K, Haass C, Steiner H, Bartenstein P, Hems J, Rominger A. Cross-sectional comparison of small animal [18F]florbetaben amyloid-PET between transgenic AD mouse models. PLoS ONE. 2015; 10(2):e0116678. [PubMed: 25706990]

Chattopadhyay S, Xue B, Pichika R, Collins D, Bagnera R, Leslie FM, Christian BT, Shi B, Narayanan TK, Potkin SG, Mukherjee J. Synthesis and evaluation of nicotine α4β 2 receptor ligand, 5-(3'-fluoropropyl)-3-(2-(*S*)-pyrrolidinyl)methoxy)pyridine (^{18}F-nifrolidine) in rodents and imaging by PET in non-human primate. J Nucl Med. 2005; 46:130–140. [PubMed: 15632043]

Coleman RA, Liang C, Patel R, Ali S, Mukherjee J. Brain and brown adipose tissue metabolism in Tg 2576 transgenic mice models of Alzheimer's disease assessed using ^{18}F-FDG PET. Mol Imag. 2017; 16:1–9.

Deane R, Bell RD, Sagare A, Zlokovic BV. Clearance of amyloid-b peptide across the blood-brain barrier: Implications for therapies in Alzheimer's disease. CNS Neurol Disord Drug Targets. 2009; 8:16–30. [PubMed: 19275634]

Doody RS, Thomas RG, Farlow MD. Phase 3 trials of solanezumab for mild-to-moderate Alzheimer's disease. N Engl J Med. 2014; 370:311–321. [PubMed: 24450890]

Filser S, Ovsepian SV, Masana M, Blazquez-Llorca L, Brandt Elvang A, Volbracht C, Muller MB, Jung CK, Hems J. Pharmacological inhibition of BACE1 impairs synaptic plasticity and cognitive functions. Biol Psych. 2015; 77:729–739.

Garcia-Alloza M, Borrelli LA, Rozkalne B, Hyman T, Bacskai BJ. Curcumin labels amyloid pathology in vivo, disrupts existing plaques, and partially restores distorted neurites in an Alzheimer's mouse model. J Neurochem. 2007; 102:1095–1104. [PubMed: 17472706]

Gerenu G, Liu K, Chojnacki JE, et al. Curcumin/melatonin hybrid 5-(4-hydroxyphenyl)-3-oxo-pentanoic acid [2-(5-meth-oxy-1H-indol-3-yl)-ethyl]-amide ameliorates AD-like pathology in the APP/PS1 mouse mode. ACS Chem Neurosci. 2015; 6:1393–1399. [PubMed: 25893520]

Hu S, Maiti P, Ma X, Jones MR, Cole GM, Frautschy SA. Clinical development of curcumin in neurodegenerative disease. Expert Rev Neurother. 2015; 15:629–637. [PubMed: 26035622]

Jessen NA, Munk AS, Lundgaard I, Nedergaard M. The glymphatic system: a beginners guide. Neurochem Res. 2015; 40:2583–2599. [PubMed: 25947369]

Krishnamurthy S, Tichenor MD, Satish AG, Lehman DB. A proposed role for efflux transporters in the pathogenesis of hydrocephalus. Croat Med J. 2014; 55:66–76.

Leinenga G, Gotz J. Scanning ultrasound removes amyloid-beta and restores memory in an Alzheimer's disease mouse model. Sci Transl Med. 2015; 7(278):278ra33.

Mancuso C, Santangelo R. Pharmacological and toxicological aspects. Food Chem Toxicol. 2014; 65:185–195. [PubMed: 24373826]

Moghbel MC, Saboury B, Basu S, Metzler SD, Torigian DA, Langstrom B, Alavi A. Amyloid-b imaging with PET in Alzheimer's disease: is it feasible with current radiotracers and technologies? Eur J Nucl Mol Imag. 2012; 39:202–208.

Mukherjee J, Lao P, Betthauser T, Samra GK, Pan ML, Patel IH, Liang C, Metherate R, Christian BT. Human brain imaging of nicotinic acetylcholine α4β 2* receptors using [18F]Nifene: selectivity, functional activity, toxicity, aging effects, gender effects and extrathalamic pathways. J Comp Neurol. 2018; 526:80–96. [PubMed: 28875553]

Pan ML, Mukherjee MT, Patel HH, Patel B, Constantinescu CC, Mirbolooki MR, Liang C, Mukherjee J. Evaluation of [^{11}C] TAZA for amyloid Aβ plaque imaging in postmortem Alzheimer's disease brain region and whole body distribution in rodent PET/CT. Synapse. 2016; 70:163–176. [PubMed: 26806100]

Pahnke J, Wolkenhauer O, Krohn M, Walker LC. Clinico-pathologic function of cerebral ABC transporters-implications for the pathogenesis of Alzheimers disease. Curr Alzheimers Res. 2008; 5:396–405.

Posadas I, Lopez-Hernandez B, Cena V. Nicotinic receptors in neurodegeneration. Curr Neuropharmacol. 2013; 11:298–314. [PubMed: 24179465]

Pichika R, Easwaramoorthy B, Christian BT, Shi B, Narayanan TK, Collins D, Mukherjee J. Nicotine α4β 2 receptor imaging agents. Part III. Synthesis and evaluation of 18F-Nifzetidine in rodents and imaging by PET in non-human primate. Nucl Med Biol. 2011; 38:1183–1192. [PubMed: 21831652]

Pichika R, Kuruvilla SA, Patel N, Vu K, Sinha S, Easwaramoorthy B, Narayanan TK, Shi B, Christian B, Mukherjee J. Nicotine α4β 2 receptor imaging agents. Part IV. Synthesis and evaluation of ^{18}F-nifrolene in rodents and non-human primate by PET imaging. Nucl Med Biol. 2013; 40:117–125. [PubMed: 23141552]

Pi R, Mao X, Chao X, Cheng Z, Liu M, Duan XX, Ye M, Chen X, Mei Z, Liu P, Li W, Han Y. Tacrine-6-ferulic acid, a novel multifunctional dimer, inhibits amyloid-β mediated Alzheimer's disease associated pathogenesis in vitro and in vivo. PLoS ONE. 2012; 7:e31921. [PubMed: 22384101]

Qosa H, Abuznait AH, Hill RA, Kaddoumi A. Enhanced brain amyloid beta clearance by rifamycin and caffeine as a possible protective mechanism against Alzheimers disease. J Alz Dis. 2012; 31:151–156.

Ryu EK, Choe YS, Lee K, Choi Y, Kim B. Curcumin and dehydrozingerone derivatives: synthesis, radiolabeling, and evaluation for β-amyloid plaque imaging. J Med Chem. 2006; 49:6111–6119. [PubMed: 17004725]

Salloway S, Sperling R, Fox NC. Bapineuzumab 301 and 302 Clinical Trial Investigators. Two phase 3 trials of bapineuzumab in mild-to-moderate Alzheimers disease. N Engl J Med. 2014; 370:322–333. [PubMed: 24450891]

Samra GK, Intskirveli I, Govind AP, Liang C, Lazar R, Green WN, Metherate R, Mukherjee J. Development of fluorescent probes for imaging α4β 2* nicotinic acetylcholine receptors. Bioorg Med Chem Lett. 2018; 28:371–377.

Schenk D, Barbour R, Dunn W, et al. Immunization with amyloid-beta attenuates Alzheimer's disease like pathology in the PDAPP mouse. Nature. 1999; 402:537–540. [PubMed: 10591214]

Siemers ER, Sundell KL, Carlson C, Case M, Sethuraman G, Liu-Seifert H, Dowsett SA, Pontecorvo MJ, Dean RA, Demattos R. Phase 3 solanezumab trials: secondary outcomes in mild Alzheimer' disease patients. Alzheimers Dement. 2016; 12:110–120. [PubMed: 26238576]

Sultana R. Ferulic acid ethyl ester as a potential therapy in neurodegenerative disease. Biochim Biophys Acta. 2012; 1822:748–752. [PubMed: 22064438]

Sgarbossa A, Giacomazza D, Di Carlo M. Ferulic acid: a hope for Alzheimer's disease therapy from plants. Nutrients. 2015; 7:5764–5782. [PubMed: 26184304]

Syvanen S, Eriksson. Advances in PET imaging of P-glycoprotein function at the blood-brain barrier. ACS Chem Neurosci. 2013; 4:225–237. [PubMed: 23421673]

Tahara H, Kusuhara H, Fuse E, Sugiyama Y. P-glycoprotein plays a major role in the efflux of fexofenadine in the small intestine and blood brain barrier, but only a limited role in its biliary excretion. Drug Metab Dis. 2005; 33:963–968.

Tampellini D. Synaptic activity and Alzheimer's disease: a critical update. Front Neurosci. 2015; 9:423. [PubMed: 26582973]

Vassar R. BACE1 inhibitor drugs in clinical trials for Alzheimer's disease. Alzheimer's Res & Ther. 2014; 6:89. [PubMed: 25621019]

Venigalla M, Sonego S, Gyengesi E, Sharman MJ, Munch G. Novel promising therapeutics against chronic inflammation and neurodegeneration in Alzheimer's disease. Neurochem Int. 2016; 95:63–74. [PubMed: 26529297]

Vlaming MLH, Lappchen T, Jansen HT, et al. PET-CT imaging with [18F]-gefitinib to measure Abcd1a/1b (P-gp) and Abcg2 (Bcrp1) mediated drug-drug interactions at the murine blood-brain barrier. Nucl Med Biol. 2015; 42:833–841. [PubMed: 26264927]

Yan J-J, Jung J-S, Kim T-K, Hasan MA, Hong C-W, Nam J-S, Song D-K. Protective effects of ferulic acid in amyloid precursor protein plus presenilin-1 transgenic mouse model of Alzheimer's disease. Biol Pharm Bull. 2013; 36:140–143. [PubMed: 23075678]

Zhao R, Kalvass C, Yanni SB, Bridges AS, Pollack GM. Fexofenadine brain exposure and the influence of blood brain barrier P-glycoprotein after fexofenadine and terfenadine administration. Drug Metab Disp. 2009; 37:529–535.

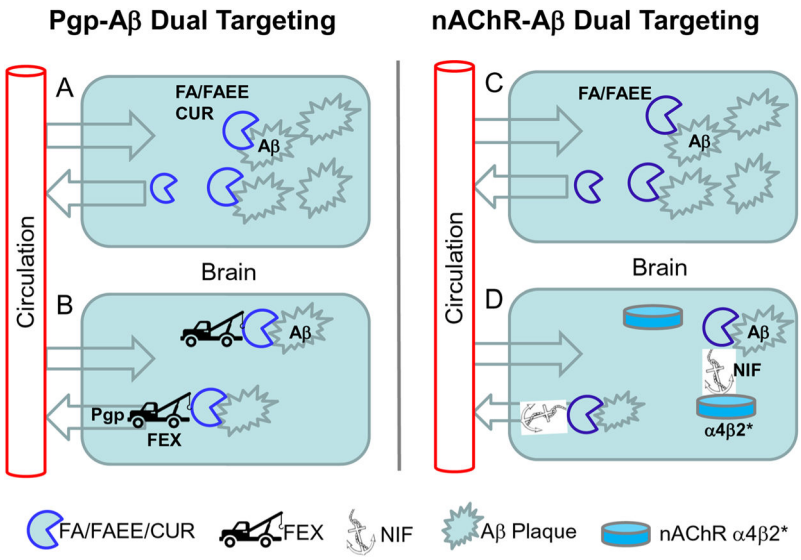

Fig. 1.

Dual agent hypothesis. **a** Aβ-binding agents, ferulic acid (FA), ferulic acid ethyl ester (FAEE), and curcumin (CUR) entering and leaving the Alzheimer's disease (AD) brain. **b** Dual agent of FA or CUR with p-glycoprotein (Pgp) substrate, fexofenadine (FEX) assist in towing the Aβ plaques out of brain and brain vasculature in the AD brain. **c** Aβ-binding agents, FA and FAEE entering and leaving the AD brain. **d** Dual agent of ferulic acid (FA) and nicotinic receptor binding agent, nifrolidine (NIF) entering the brain and NIF acting as an anchor to prolong effects of FA in the AD brain

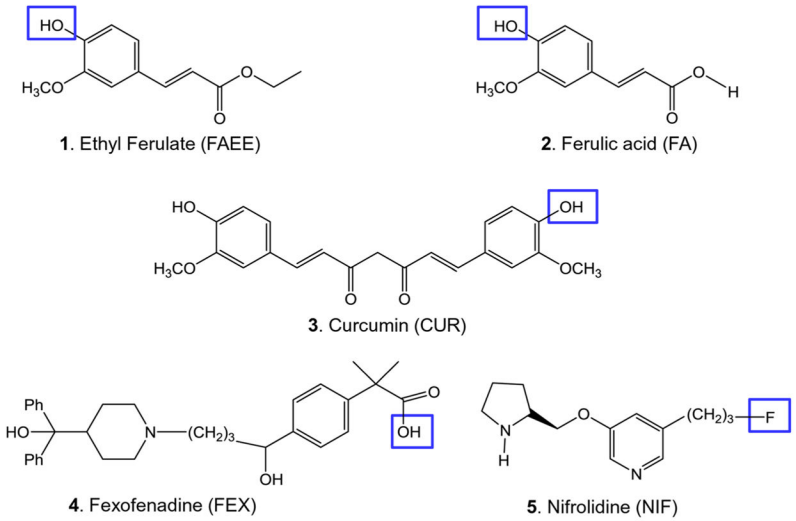

Fig. 2.

Chemical structures of compounds used. Amyloid β-binding agents, ferulic acid ethyl ester (FAEE) **1**, ferulic acid **2**, curcumin **3**, P-glycoprotein substrate fexofenadine **4**, α4β 2* nicotinic acetylcholinergic receptor agent, nifrolidine **5**. Blue boxes show the functional groups used to make the dual agents

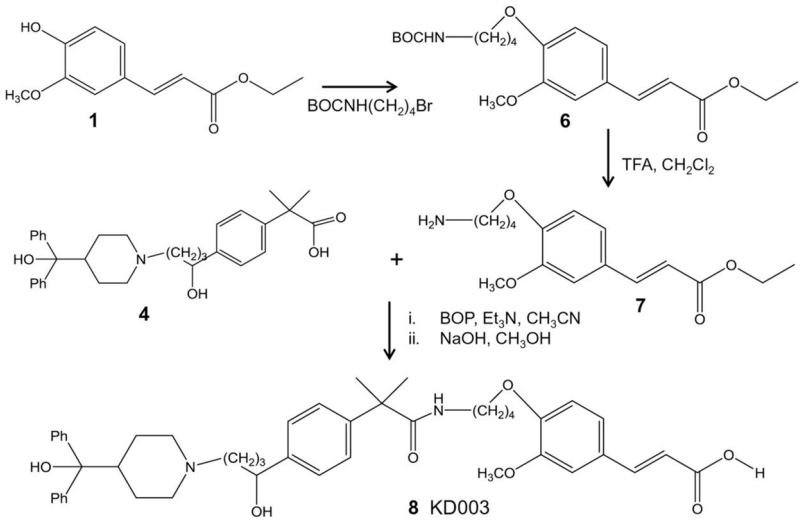

Fig. 3.

Synthesis of Aβ-Pgp agents using linker. *O*-alkylation of FAEE **1** with *N*-BOC bromobutylamine to **6**. Deprotection of *N*-BOC **6** with TFA, trifluoroacetic acid for **7**. Amide formation with FEX **4** and **7** using BOP, benzotriazol-1-yloxy)tris(dimethylamino) phosphonium hexafluorophosphate followed by base hydrolysis to provide **8**

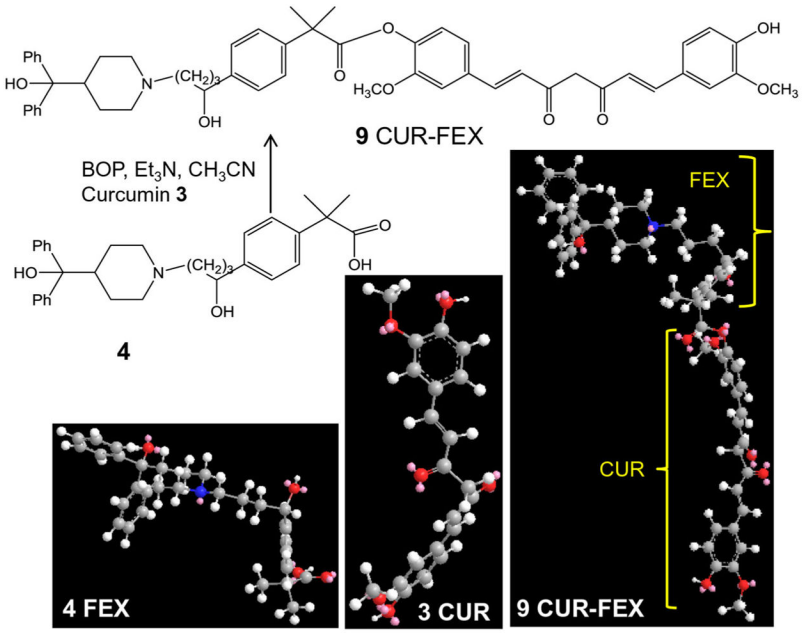

Fig. 4.

Curcumin ester synthesis of Aβ-Pgp agent. Esterification of CUR **3** and FEX **4** using BOP. Energy-minimized models comparing the dual agent, CUR-FEX **9** with CUR **3** and FEX **4**

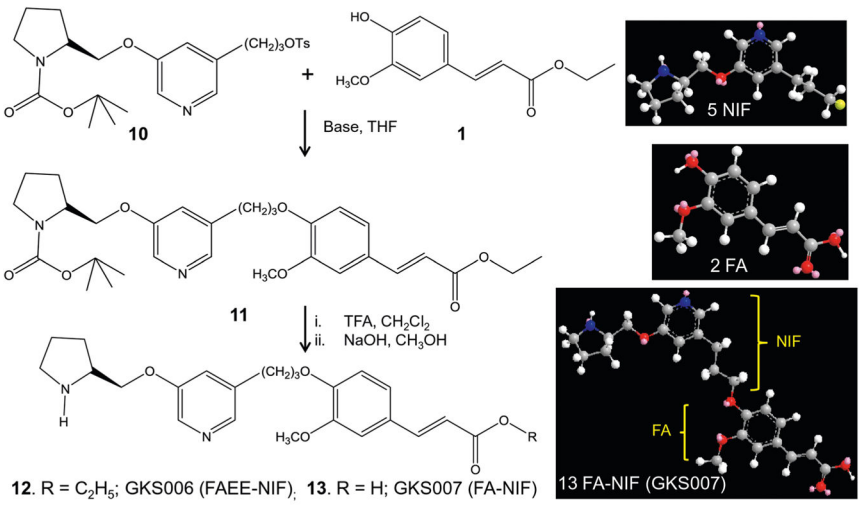

Fig. 5.

Ferulic acid ether synthesis of Aβ-α4β 2* agents. Reaction of substituted tosylate **10** and FAEE **1** (base, THF, tetrahydrofuran) to provide ether **11**. Deprotection of *N*-BOC **11** with TFA for GKS-006 **12** and base hydrolysis of **12** to provide GKS-007 **13**. Energy-minimized models comparing the dual agent, FA-NIF (GKS-007) **13** with FA **2** and NIF **5**

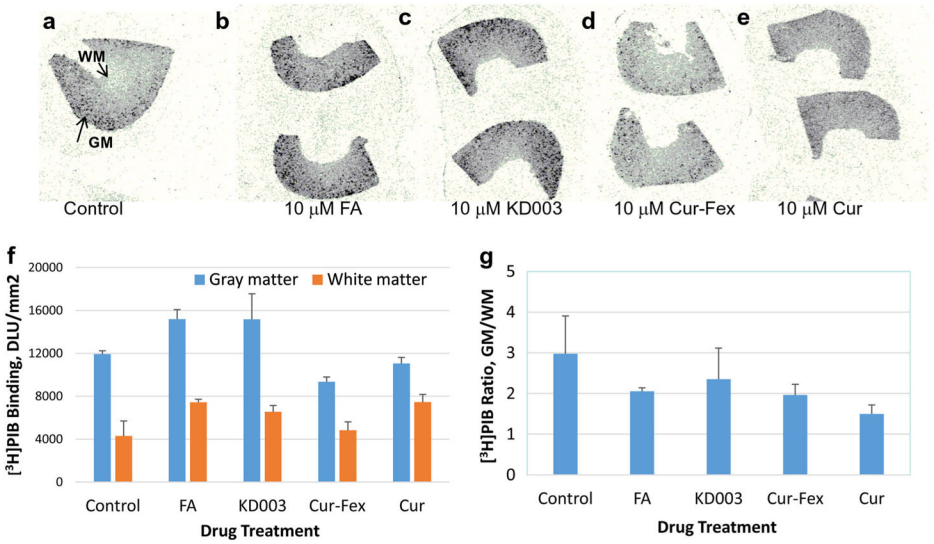

Fig. 6.

Human amyloid plaque binding of Aβ-Pgp agents. **a** Human AD brain frontal cortex autoradiograph, 10 μm thick showing gray matter (GM) and white matter (WM) binding of [^{3}H]PIB autoradiograph. **b**–**e** [^{3}H]PIB autoradiographs in adjacent brain slices in the presence of 10 μM FA, KD-003, CUR-FEX and CUR, respectively. **f** Quantitation of [^{3}H]PIB in GM and WM regions in experiments **a**–**e. g** Ratio of GM to WM in experiments **a**–**e**

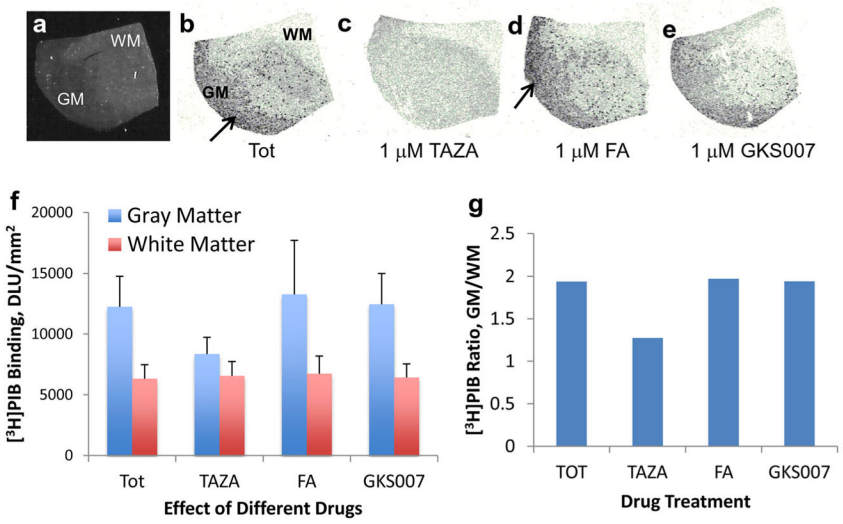

Fig. 7.

Human amyloid plaque binding of Aβ-nAChR agents. **a** Scan of 10 μm thick human AD brain frontal cortex, showing gray matter (GM) and white matter (WM). **b** [^{3}H]PIB autoradiograph in the brain slice showing GM (arrow) and WM. **c**–**e** [^{3}H]PIB autoradiographs in adjacent brain slices in the presence of 1 μM TAZA, FA and GKS-007, respectively. **f** Quantitation of [^{3}H]PIB in GM and WM regions in experiments **b**–**e. g** Ratio of GM to WM in experiments **b**–**e**

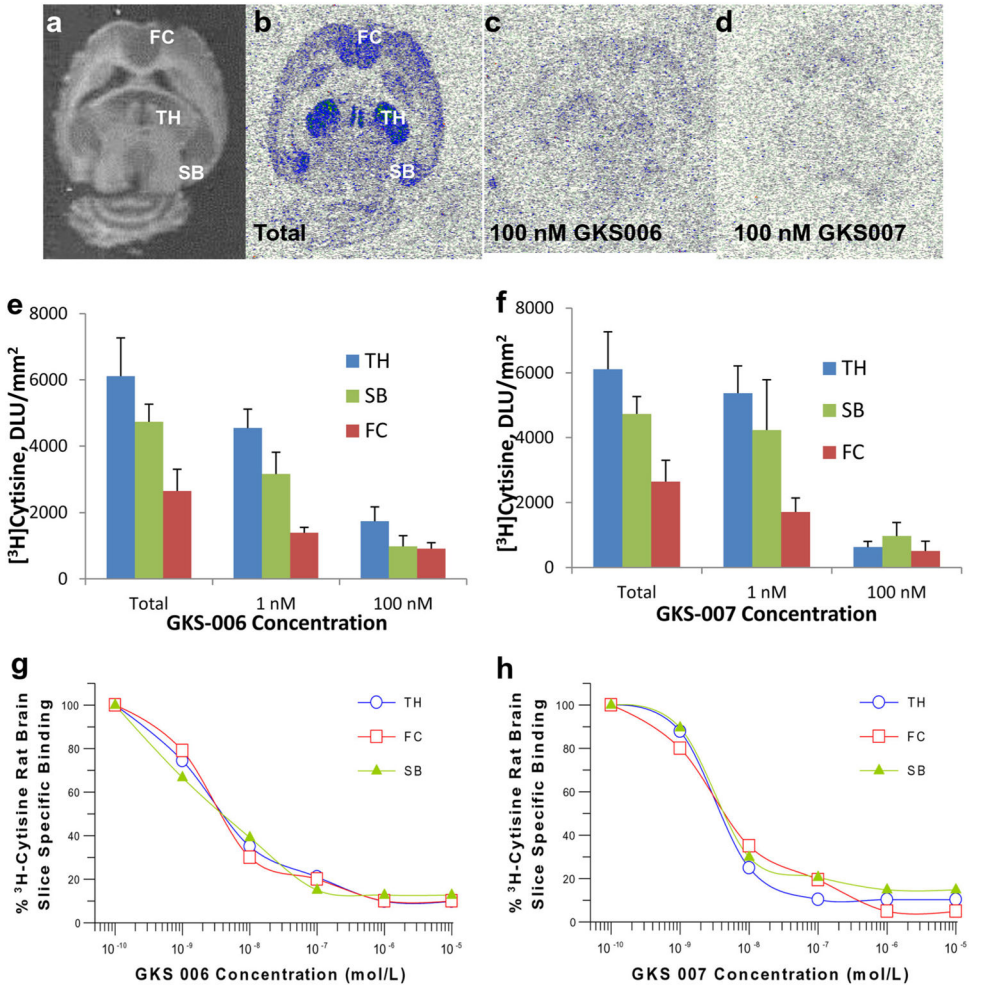

Fig. 8.

Rat brain nicotine receptor binding of Aβ-α4β 2* agents. **a** Scan of 10 μm thick rat brain slice; **b** Total binding autoradiograph of [^{3}H] cytisine in different brain regions (FC frontal cortex, SB subiculum, TH thalamus); **c** Autoradiograph of [^{3}H]cytisine in the presence of 100 nM GKS-006; **d** Autoradiograph of [^{3}H]cytisine in the presence of 100 nM GKS-007; **e** Displacement of [^{3}H]cytisine in the presence of 1 nM and 100 nM GKS-006. **f** Displacement of [^{3}H]cytisine in the presence of 1 nM and 100 nM GKS-007. **g** Competition specific binding curves of GKS-006 with [^{3}H]cytisine binding in rat brain regions shown in **b. h** Competition specific binding curves of GKS-007 with [^{3}H]cytisine binding in rat brain regions shown in **b**

Table 1

Brief summary of therapeutic agents being used Alzheimer's disease (human and animal models)

# Therapeutic agent	Target	Subjects	Outcome	Current status/references
1 AChEI, memantine	Acetylcholine levels; NMDA receptors	All stages	Lessen symptoms of memory loss and confusion	Currently FDA approved (Aricept, Razadyne,
2 Bapineuzumab	Anti-amyloid β monoclonal antibody	Mild to moderate AD	Did not improve clinical outcomes	[7]Salloway et al. 2014; research use
3 Other antibodies (solanezumab)	Anti-amyloid β monoclonal antibody	Mild to moderate AD	Did not improve clinical outcomes. Trials continue in early stage of disease	[8]Doody et al. 2014; [9]Siemers et al. 2016. Trials continue
4 Secretase inhibitors	β-secretase enzymes to reduce Aβ peptide	MCI, AD and rodent models	Liver toxicity; impaired cognition in animals	[10]Filser et al. 2015. [11]Vassar 2014 other trials continue
5 Curcumin analogs	Aβ Plaques	Transgenic mice; human AD	Mice studies promising in reducing Aβ plaques; human outcome uncertain	[12]Hu et al. 2015; [13]Gerenu et al. 2015. Studies ongoing
6 Ultrasound	Blood–brain barrier (BBB) opening	Transgenic mice	Decrease in brain Aβ plaques; improved memory task	[15]Leinenga and Gotz, 2015. Translation to humans uncertain.